Pälike, H., Lyle, M., Nishi, H., Raffi, I., Gamage, K., Klaus, A., and the Expedition 320/321 Scientists
Proceedings of the Integrated Ocean Drilling Program, Volume 320/321

Data report: Monte Carlo correlation of sediment records from core and downhole log measurements at Sites U1337 and U1338 (IODP Expedition 321)[1]

Alberto Malinverno[2]

Chapter contents

Abstract

Site-to-site lithostratigraphic correlations are vital to building a composite record of equatorial Pacific sediment and constructing a common timescale. The work described here is aimed at establishing a detailed lithostratigraphic correlation between Sites U1337 and U1338 (Integrated Ocean Drilling Program Expedition 321) on the basis of high-resolution bulk density measurements from cores and downhole logs. Using both core and log measurements best constrains site-to-site correlations, but these two data types are measured on different depth scales. Reconciling these different depth scales requires a detailed correlation to precisely align the high-resolution core and log records at each site.

This study uses an automated Monte Carlo algorithm to align core and log records at the same site and to determine site-to-site correlations. The distinguishing feature of the method is that it does not produce a single optimal correlation, but rather a sample of possible correlations that give a good match. The average of the samples gives the best correlation, and their variability measures the uncertainty inherent to the correlation.

The Monte Carlo method is first applied to correlate core splice and downhole log data at each site, so that the data can be referred to the same depth scale. The resulting correlation is close to a uniform 11%–12% expansion of the composite core depth scale, but local differences up to several meters mean that a detailed correlation is necessary to match small-scale sedimentary features. Once the downhole log data are placed onto the core depth scale, consistent site-to-site correlations between Sites U1337 and U1338 are determined by matching core and log data.

Introduction

Sediments deposited in the equatorial Pacific Ocean store some of the best long-term records of Earth's climate. These sediments record ocean-wide variations, as shown by the observation that in this region sediment physical properties correlate over large distances (Moore and Pälike, 2006). These lithostratigraphic correlations complement bio-, chemo-, and magnetostratigraphic correlations and assist in the construction of a common timescale. Integrated Ocean Drilling Program (IODP) Expeditions 320 and 321 (Pacific Equatorial Age Transect) sampled the sediment

[1]Malinverno, A., 2013. Data report: Monte Carlo correlation of sediment records from core and downhole log measurements at Sites U1337 and U1338 (IODP Expedition 321). *In* Pälike, H., Lyle, M., Nishi, H., Raffi, I., Gamage, K., Klaus, A., and the Expedition 320/321 Scientists, *Proc. IODP,* 320/321: Tokyo (Integrated Ocean Drilling Program Management International, Inc.).
doi:10.2204/iodp.proc.320321.207.2013
[2]Lamont-Doherty Earth Observatory of Columbia University, PO Box 1000, 61 Route 9W, Palisades NY 10964-1000, USA.
alberto@ldeo.columbia.edu

mound deposited near the paleoequator to validate and extend the astronomical calibration of the Cenozoic geologic timescale and to improve, date, and intercalibrate stratigraphic datums (see the **"Expedition 320/321 summary"** chapter [Pälike et al., 2010]).

This data report applies a Monte Carlo method to obtain a detailed lithostratigraphic correlation by matching two sediment records. The distinguishing feature of the method is that it does not produce a single optimal correlation, but rather a sample of possible correlations that result in a good match. The average of these samples gives the best correlation, and their variability measures the uncertainty that is inherent to the correlation, highlighting intervals where the match is relatively poor and the correlation less reliable.

The method is applied to high-resolution bulk density measurements from core samples and downhole logs from Expedition 321 Sites U1337 and U1338, which targeted the early Miocene to present time interval and were drilled 600 km apart (see the **"Expedition 320/321 summary"** chapter [Pälike et al., 2010]). A combination of core and log measurements best constrains site-to-site correlations, but complications occur because these two data types are placed on different depth scales. The cumulative length of drill pipe is used for core depth, whereas the measured length of the wireline cable determines depth in downhole logs. Moreover, to obtain as complete a record as possible, a composite depth scale is constructed by splicing core sections taken from different holes at the same site. This process typically expands the actual thickness of the cored interval by 10%–15% (Lisiecki and Herbert, 2007; **Westerhold et al.,** 2012). Reconciling these different depth scales requires a detailed correlation to precisely align the high-resolution core and log records at each site prior to site-to-site correlation. The Monte Carlo method is applied to first correlate core and downhole log data at each site, so that all data are placed on the same depth scale. Core and downhole log data are then used to obtain a reliable lithostratigraphic correlation between the two sites.

Materials and methods

Core and downhole log data

The data used here consist of density core splices and downhole log data obtained at Sites U1337 and U1338. The density core splices were obtained from gamma ray attenuation (GRA) densities measured on whole-round core sections on the R/V *JOIDES Resolution*. The splices were painstakingly constructed by overlapping GRA density records from three holes at each site (**Wilkens et al.,** in press). The downhole density log data were measured using the Schlumberger Hostile Environment Litho-Density Sonde (HLDS) wireline logging tool in Holes U1337A and U1338B.

The core splice and downhole log data have different depth coverages and measurement resolutions. Although the core splices span the full interval drilled, there are no downhole log data from the top of the hole. This is because the drill pipe is typically lowered to ~80 meters below seafloor (mbsf) during logging to avoid the near-seafloor interval where the borehole is enlarged and irregular. The GRA data have a nominal resolution of <1 cm (measurements were taken every 2.5 cm), whereas the downhole density log has a vertical resolution of ~20 cm. Detailed comparisons, however, show that the difference in resolution is minor and that the decimeter-scale sedimentary features that are most useful for correlation are usually well resolved in both data sets. More details on the GRA and log measurements are in the **"Methods"** chapter (Expedition 320/321 Scientists, 2010).

A major complication that prevents immediate correlation of core splice and downhole log data is that they are referred to different depth scales. The current IODP terminology (**www.iodp.org/doc_download/3171-iodpdepthscaleterminologyv2**) defines the depth scale of the core splices as composite core depth below seafloor (CCSF) and the depth scale of the processed downhole logs as wireline matched depth below seafloor (WMSF). The CCSF depth scale is determined starting from the seafloor by splicing the GRA density records measured in different core sections from different holes. The WMSF depth scale is determined by referring the depth measured by the wireline cable length to the seafloor (typically defined by a step change in the natural gamma radiation log). The wireline depths measured in different logging runs are then "matched" by small adjustments that align the natural gamma radiation log acquired in each run.

Reversible jump Monte Carlo sampling

The process of determining a mapping function that relates depth in one record to depth in another is illustrated in Figure **F1.** Solutions in the literature include the nonlinear optimization methods of Martinson et al. (1982) and Brüggemann (1992) and the exhaustive search method of Lisiecki and Lisiecki (2002). Whereas these approaches focus on obtaining an optimal result, the Monte Carlo method described here also quantifies the uncertainty of the inferred mapping function. The mapping function will have a large uncertainty in intervals where the match between the records remains poor while the mapping function can vary significantly. This measure of uncertainty is important to quantify the accuracy of the correlation.

For comparison, the two records are rescaled to zero mean and unit standard deviation and their match is measured by a residual standard deviation (the standard deviation of the difference between the records). The mapping function is defined at any depth by linear interpolation between a number of nodes (Fig. **F1**). The problem is then to determine sets of nodes that give a good match between the two records (i.e., a small residual standard deviation). An additional requirement is that the gradient of the mapping function should not contain large fluctuations (Brüggemann, 1992; Lisiecki and Lisiecki, 2002). In the context of this study, large changes in the gradient of the mapping function would correspond to unrealistic measured depth errors (for core-log correlations at the same site) or excessive differences in sedimentation rate (for correlations between sites).

The requirements of a smooth mapping function and of a good data match can be combined in a Bayesian formulation, which defines a prior distribution and a likelihood of the mapping function. The value of the prior will be higher for mapping functions whose gradients have smaller fluctuations about their average. Mapping functions that result in closer matches between the records will have a higher value of likelihood. The posterior distribution of mapping functions is proportional to the product of prior and likelihood and balances the competing requirements of a smooth mapping function and of a close match of the records. This Bayesian formulation has been widely used in geophysical inverse problems (Tarantola and Valette, 1982; Jackson and Matsu'ura, 1985; Duijndam, 1988; Tarantola, 2005) and has been applied to cycle stratigraphy (Malinverno et al., 2010) and timescale construction (Malinverno et al., 2012).

A key feature of the correlation problem in Figure **F1** is that the number of nodes in the mapping function is one of the unknowns. In the apt terminology of Sambridge et al. (2006), this is a "trans-dimensional" inverse problem. Green (1995) devised a general algorithm that can be applied to these problems, called reversible jump Markov chain Monte Carlo sampling. In the correlation problem treated here, the reversible jump algorithm begins from a starting set of nodes that define an initial approximate correlation and continues as follows:

1. Propose a "candidate" mapping function by
   - Perturbing the coordinates of an existing node,
   - Adding a new node, or
   - Deleting an existing node (except for the starting nodes).
2. Accept or reject the candidate mapping function on the basis of its posterior probability as in the Metropolis-Hastings algorithm (Metropolis et al., 1953; Hastings, 1970). The posterior probability is higher for mapping functions that
   - Result in a better match (i.e., a smaller residual standard deviation) and
   - Have smaller fluctuations in their gradient.
3. Repeat from step 1.

This simple algorithm asymptotically draws samples from the posterior distribution of mapping functions. For examples of reversible jump sampling applied to geophysical inverse problems, see Malinverno (2002), Malinverno and Leaney (2005), Sambridge et al. (2006), Bodin and Sambridge (2009), and Piana Agostinetti and Malinverno (2010).

A sequence of 2000 sampling iterations of the reversible jump algorithm is shown in Figure **F2.** The residual standard deviation, which measures how close the match is between the two records, decreases as sampling progresses and becomes nearly constant after ~1000 iterations. The likelihood function correspondingly increases. On the other hand, the value of the prior distribution decreases, mostly because the number of nodes in the mapping function increases to achieve a better data match. The decrease in the prior distribution is compensated by a much larger increase in the likelihood, meaning that the cost of adding more nodes is much less than the gain because of better data matching so that the posterior probability of the mapping function increases during the sampling.

The likelihood function and the prior distribution are controlled by target standard deviations of the data residuals and of the mapping function gradient, respectively. The relative size of these target standard deviations will weigh the competing needs of matching the data and minimizing changes in the mapping function gradient. The target standard deviation of the data residuals is set to be one of the unknown parameters as in a hierarchical Bayes formulation (Malinverno and Briggs, 2004). This means that this target standard deviation does not need to be predetermined; the algorithm samples it by iteratively perturbing its value and effectively adjusts it to match the actual residual standard deviation achieved by the sampling (Fig. F2). Numerical experiments showed that a target standard deviation of the mapping function gradient equal to 20% of the mean gradient resulted in a reasonable trade-off between data match and smoothness of the mapping function.

The results described below were all obtained from 100 independent runs of the reversible jump algorithm. Each run consisted of 2000 sampling iterations. The mean mapping function and its standard deviation were determined from the 100 mapping functions obtained at the end of each run. This multiple run strategy minimizes the effect of sampling secondary modes of the posterior distribution. Although the Monte Carlo method will asymptotically sample the global mode of the posterior distribution, the sampling can still remain for a large number of iterations in a secondary mode.

Results

Correlations within Sites U1337 and U1338

The first step is to correlate core splices and downhole logs at Sites U1337 and U1338 so that both records can be placed on the same depth scale (Fig. F1). The Monte Carlo sampling started from eight nodes at Site U1337 and four nodes at Site U1338. These starting nodes were chosen to match major features in the two records; in particular, they correlate a thin 16–40 cm chert interval that was imaged in the downhole logs and that had poor core recovery. This distinctive "baby chert" was located at 240 m WMSF at Site U1337 and 281.6 m WMSF at Site U1338 (see Fig. F47 in the "Expedition 320/321 summary" chapter [Pälike et al., 2010]).

The estimated mapping functions are close to a constant expansion of the composite core depth scale that is ~12% at Site U1337 and ~11% at Site U1338 (Figs. F3, F4). These values are consistent with the 9%–16% composite depth scale expansions determined for Expedition 320 Sites U1331–U1334 by Westerhold et al. (2012). However, differences between the estimated mapping functions and constant core expansion reach about ±5 m at Site U1337 and ±2 m at Site U1338 (Figs. F3, F4). Although the magnitude of these differences is not the same, the overall pattern is similar at the two sites. A possible explanation may be lithology variations. The shallower half of the interval drilled at both sites contains a sizable siliceous component, whereas the deeper half is dominated by calcareous nannofossil ooze grading downward to chalk. These different lithologies may result in different core expansions. On the other hand, these differences are relative to the downhole log depth scale, which may itself be affected by errors (e.g., due to stretching of the wireline cable). Whatever the cause, results in Figures F3 and F4 show that a detailed correlation that goes beyond a constant core expansion is necessary to match small-scale features in the core and downhole log data.

Figures F5 and F6 show the close match of core splice and downhole log data that is achieved when both records are put on the same depth scale. The match is generally excellent, with the exception of the deepest intervals below ~350 m WMSF or ~400 m CCSF. Density variations are smaller in these deep intervals, making correlations more ambiguous. Also, in the deeper hole intervals, core recovery was lower and core conditions were poorer, making the splice data less robust. Outside of these deep intervals, the uncertainties of the mapping functions are generally <1 m (1 standard deviation; Figs. F3, F4).

Correlations between Sites U1337 and U1338

Figures F7 and F8 show the results of correlating core splice data and downhole log data between Sites U1337 and U1338. To obtain correlations that could be directly compared, the downhole log data were placed on the composite core depth scale (CCSF) using the mapping functions obtained previously (Figs. F3, F4). The Monte Carlo sampling started from six nodes for the core splice correlation and four nodes for the downhole log correlation. The site-to-site mapping functions obtained for core splice and downhole log data are illustrated in Figure F9. Once the two data sets are placed on the same depth scale, the site-to-site correlations are entirely consistent.

These lithostratigraphic correlations have the smallest uncertainties in the intervals 130–330 m CCSF at Site U1337 and 140–380 m CCSF at Site U1338. In these intervals, the match of small-scale features in the two records is excellent (Figs. F7, F8). The uncertainties of the mapping function outside this well-correlated interval reach several meters (1 standard deviation; Fig. F9). These uncertainties quantify the confidence of correlations based on lithostratigraphy. For example, a stratigraphic event observed at 400 m CCSF at Site U1338 can be correlated to a depth of 346 m CCSF at Site U1337, but this correlation has an inherent uncertainty of about ±5 m (1 standard deviation). To assist in building a composite sedimentary record in the equatorial Pacific Ocean, the mapping functions that correlate Sites U1337 and U1338 (Fig. F9) are provided in Table T1 (core splice data) and Table T2 (downhole log data).

Acknowledgments

This research was supported by grant JOI-T321A31 of the U.S. Science Support Program and used samples and data provided by the Integrated Ocean Drilling Program. The efforts of the *JOIDES Resolution* shipboard and drilling personnel and of the science parties of IODP Expeditions 320 and 321 are gratefully acknowledged. Special thanks to Roy Wilkens for providing the core density splice data used in this study.

References

Bodin, T., and Sambridge, M., 2009. Seismic tomography with the reversible jump algorithm. *Geophys. J. Int.,* 178(3):1411–1436. **doi:10.1111/j.1365-246X.2009.04226.x**

Brüggemann, W., 1992. A minimal cost function method for optimizing the age-depth relation of deep-sea sediment cores. *Paleoceanography,* 7(4):467–487. **doi:10.1029/92PA01235**

Duijndam, A.J.W., 1988. Bayesian estimation in seismic inversion, Part I: Principles. *Geophys. Prosp.,* 36(8):878–898. **doi:10.1111/j.1365-2478.1988.tb02198.x**

Expedition 320/321 Scientists, 2010. Methods. *In* Pälike, H., Lyle, M., Nishi, H., Raffi, I., Gamage, K., Klaus, A., and the Expedition 320/321 Scientists, *Proc. IODP,* 320/321: Tokyo (Integrated Ocean Drilling Program Management International, Inc.). **doi:10.2204/iodp.proc.320321.102.2010**

Green, P.J., 1995. Reversible jump Markov chain Monte Carlo computation and Bayesian model determination. *Biometrika,* 82(4):711–732. **doi:10.1093/biomet/82.4.711**

Hastings, W.K., 1970. Monte Carlo sampling methods using Markov chains and their applications. *Biometrika,* 57(1):97–109. **doi:10.1093/biomet/57.1.97**

Jackson, D.D., and Matsu'ura, M., 1985. A Bayesian approach to nonlinear inversion. *J. Geophys. Res., [Solid Earth],* 90(B1):581–591. **doi:10.1029/JB090iB01p00581**

Lisiecki, L.E., and Herbert, T.D., 2007. Automated composite depth scale construction and estimates of sediment core extension. *Paleoceanography,* 22(4):PA4213. **doi:10.1029/2006PA001401**

Lisiecki, L.E., and Lisiecki, P.A., 2002. Application of dynamic programming to the correlation of paleoclimate records. *Paleoceanography,* 17(4):1049. **doi:10.1029/2001PA000733**

Malinverno, A., 2002. Parsimonious Bayesian Markov chain Monte Carlo inversion in a nonlinear geophysical problem. *Geophys. J. Int.,* 151(3):675–688. **doi:10.1046/j.1365-246X.2002.01847.x**

Malinverno, A., and Briggs, V.A., 2004. Expanded uncertainty quantification in inverse problems: hierarchical Bayes and empirical Bayes. *Geophysics,* 69(4):1005–1016. **doi:10.1190/1.1778243**

Malinverno, A., Erba, E., and Herbert, T.D., 2010. Orbital tuning as an inverse problem: chronology of the early Aptian oceanic anoxic Event 1a (Selli Level) in the Cismon APTICORE. *Paleoceanography,* 25(2):PA2203. **doi:10.1029/2009PA001769**

Malinverno, A., Hildebrandt, J., Tominaga, M., and Channell, J.E.T., 2012. M-sequence geomagnetic polarity time scale (MHTC12) that steadies global spreading rates and incorporates astrochronology constraints. *J. Geophys. Res., [Solid Earth],* 117(B6):B06104. **doi:10.1029/2012JB009260**

Malinverno, A., and Leaney, W.S., 2005. Monte-Carlo Bayesian look-ahead inversion of walkaway vertical seismic profiles. *Geophys. Prosp.,* 53(5):689–703. **doi:10.1111/j.1365-2478.2005.00496.x**

Martinson, D.G., Menke, W., and Stoffa, P., 1982. An inverse approach to signal correlation. *J. Geophys. Res., [Solid Earth],* 87(B6):4807–4818. **doi:10.1029/JB087iB06p04807**

Metropolis, N., Rosenbluth, A.W., Rosenbluth, M.N., Teller, A.H., and Teller, E., 1953. Equation of state calculations by fast computing machines. *J. Chem. Phys.,* 21(6):1087–1092. **doi:10.1063/1.1699114**

Moore, T., and Pälike, H., 2006. Time is of the essence. *Oceanography,* 19(4):22–27. **doi:10.5670/oceanog.2006.01**

Pälike, H., Nishi, H., Lyle, M., Raffi, I., Gamage, K., Klaus, A., and the Expedition 320/321 Scientists, 2010. Expedition 320/321 summary. *In* Pälike, H., Lyle, M., Nishi, H., Raffi, I., Gamage, K., Klaus, A., and the Expedition 320/321 Scientists, *Proc. IODP,* 320/321: Tokyo (Integrated Ocean Drilling Program Management International, Inc.). **doi:10.2204/iodp.proc.320321.101.2010**

Piana Agostinetti, N., and Malinverno, A., 2010. Receiver function inversion by trans-dimensional Monte Carlo sampling. *Geophys. J. Int.,* 181(2):858–872. **doi:10.1111/j.1365-246X.2010.04530.x**

Sambridge, M., Gallagher, K., Jackson, A., and Rickwood, P., 2006. Trans-dimensional inverse problems, model comparison, and the evidence. *Geophys. J. Int.,* 167(2):528–542. **doi:10.1111/j.1365-246X.2006.03155.x**

Tarantola, A., 2005. *Inverse Problem Theory and Methods for Model Parameter Estimation:* Philadelphia (Soc. Ind. Appl. Math.). **doi:10.1137/1.9780898717921**

Tarantola, A., and Valette, B., 1982. Inverse problems = quest for information. *J. Geophys.,* 50:159–170. **http://www.ipgp.fr/~tarantola/Files/Professional/Papers_PDF/IP_QI_original.pdf**

Westerhold, T., Röhl, U., Wilkens, R., Pälike, H., Lyle, M., Jones, T.D., Bown, P., Moore, T., Kamikuri, S., Acton, G., Ohneiser, C., Yamamoto, Y., Richter, C., Fitch, P., Scher, H., Liebrand, D., and the Expedition 320/321 Scientists, 2012. Revised composite depth scales and integration of IODP Sites U1331–U1334 and ODP Sites 1218–1220. *In* Pälike, H., Lyle, M., Nishi, H., Raffi, I., Gamage, K., Klaus, A., and the Expedition 320/321 Scientists, *Proc. IODP,* 320/321: Tokyo (Integrated Ocean Drilling Program Management International, Inc.). doi:10.2204/iodp.proc.320321.201.2012

Wilkens, R.H., Dickens, G.R., Tian, J., Backman, J., and the Expedition 320/321 Scientists, in press. Data report: revised composite depth scales for Sites U1336, U1337, and U1338. *In* Pälike, H., Lyle, M., Nishi, H., Raffi, I., Gamage, K., Klaus, A., and Expedition 320/321 Scientists, *Proc. IODP,* 320/321: Tokyo (Integrated Ocean Drilling Program Management International, Inc.).

Initial receipt: 21 June 2012
Acceptance: 14 December 2012
Publication: 19 February 2013
MS 320321-207

Figure F1. A spliced core density record (red) can be closely correlated to a downhole density log (black); correlations of discrete features are shown by dashed gray lines. The conversion between core depth and log depth is given by a mapping function (thick gray curve) defined by a few nodes (gray dots).

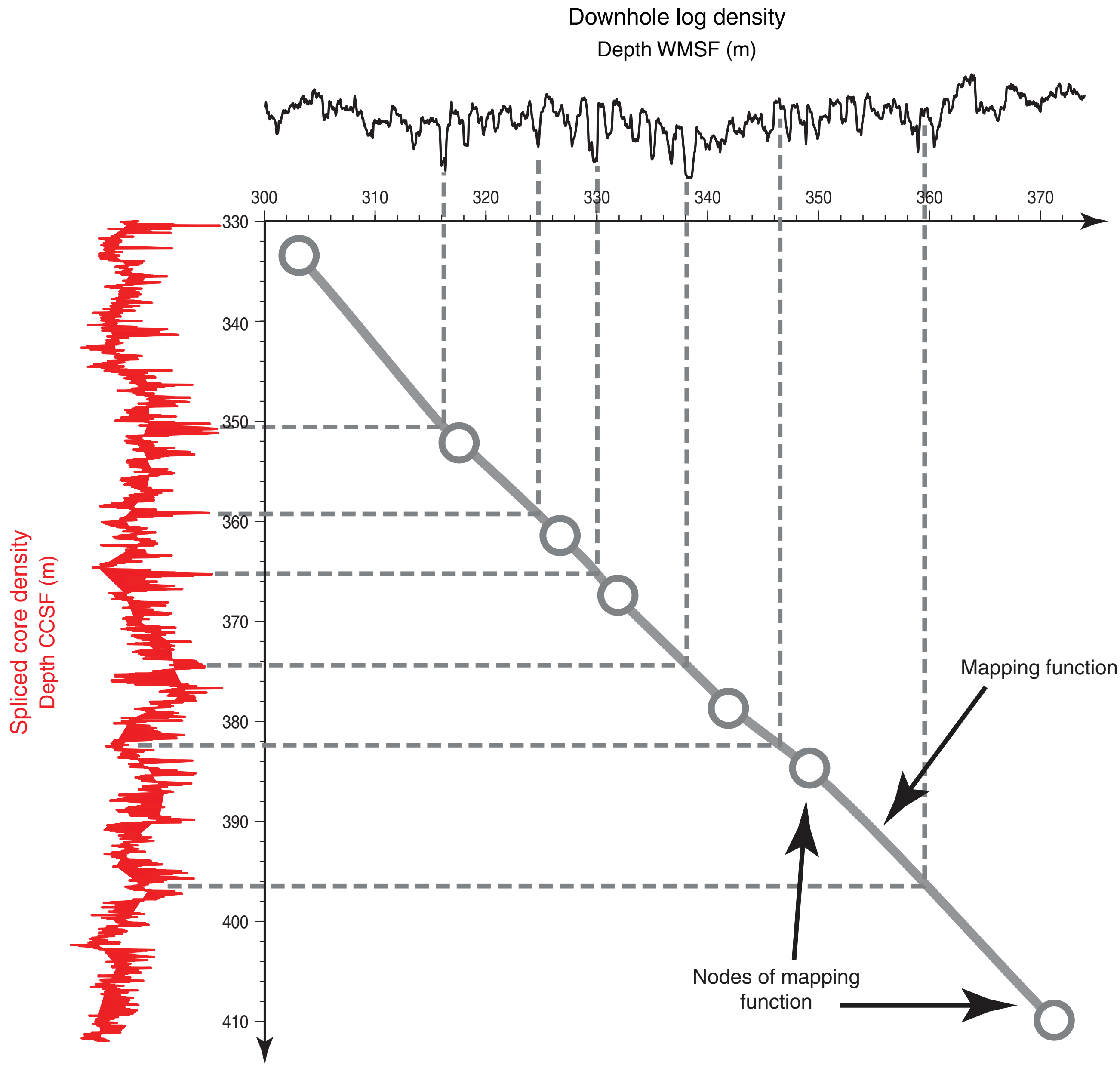

Figure F2. Progress of the reversible jump Monte Carlo algorithm in 2000 iterations. The residual standard deviation, which measures the mismatch between the two records, progressively decreases and the likelihood correspondingly increases. The red line shows the value of the target residual standard deviation, which is one of the unknown parameters and is adjusted by the algorithm during sampling. The value of the prior distribution decreases as the number of nodes necessary to improve the match between the two records increases.

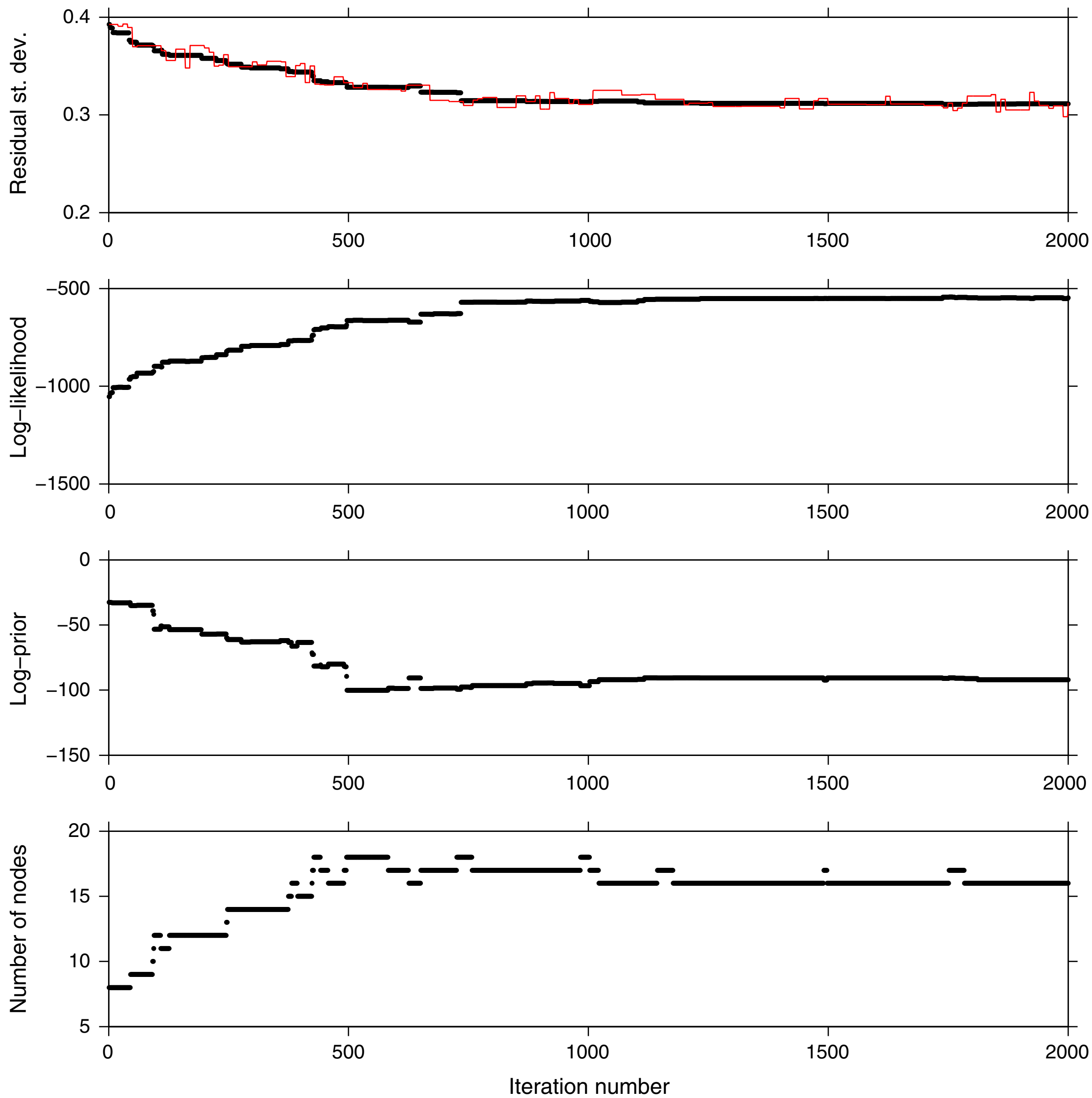

Figure F3. Mapping function between core splice and downhole log data (top) and residual of mapping function over the average core expansion (bottom) at Site U1337. The average mapping function is shown by a thick red line, and uncertainty bounds (±1 standard deviation) by thin red lines. The thick blue dashed line shows the average core expansion, and the gray dots are the starting nodes for the correlation.

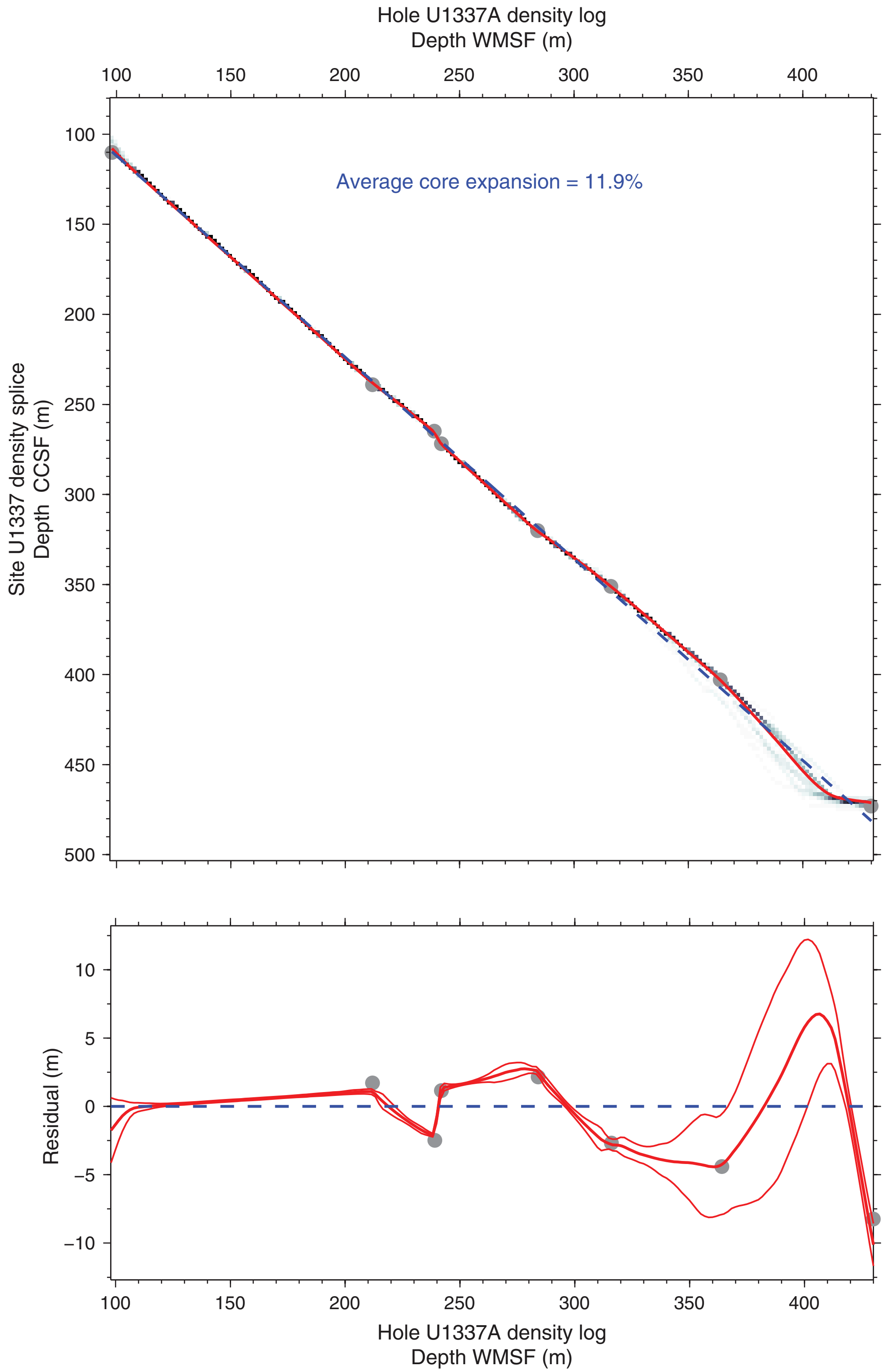

Figure F4. Mapping function between core splice and downhole log data (top) and residual of mapping function over the average core expansion (bottom) at Site U1338. The average mapping function is shown by a thick red line, and uncertainty bounds (±1 standard deviation) by thin red lines. The thick blue dashed line shows the average core expansion, and the gray dots are the starting nodes for the correlation.

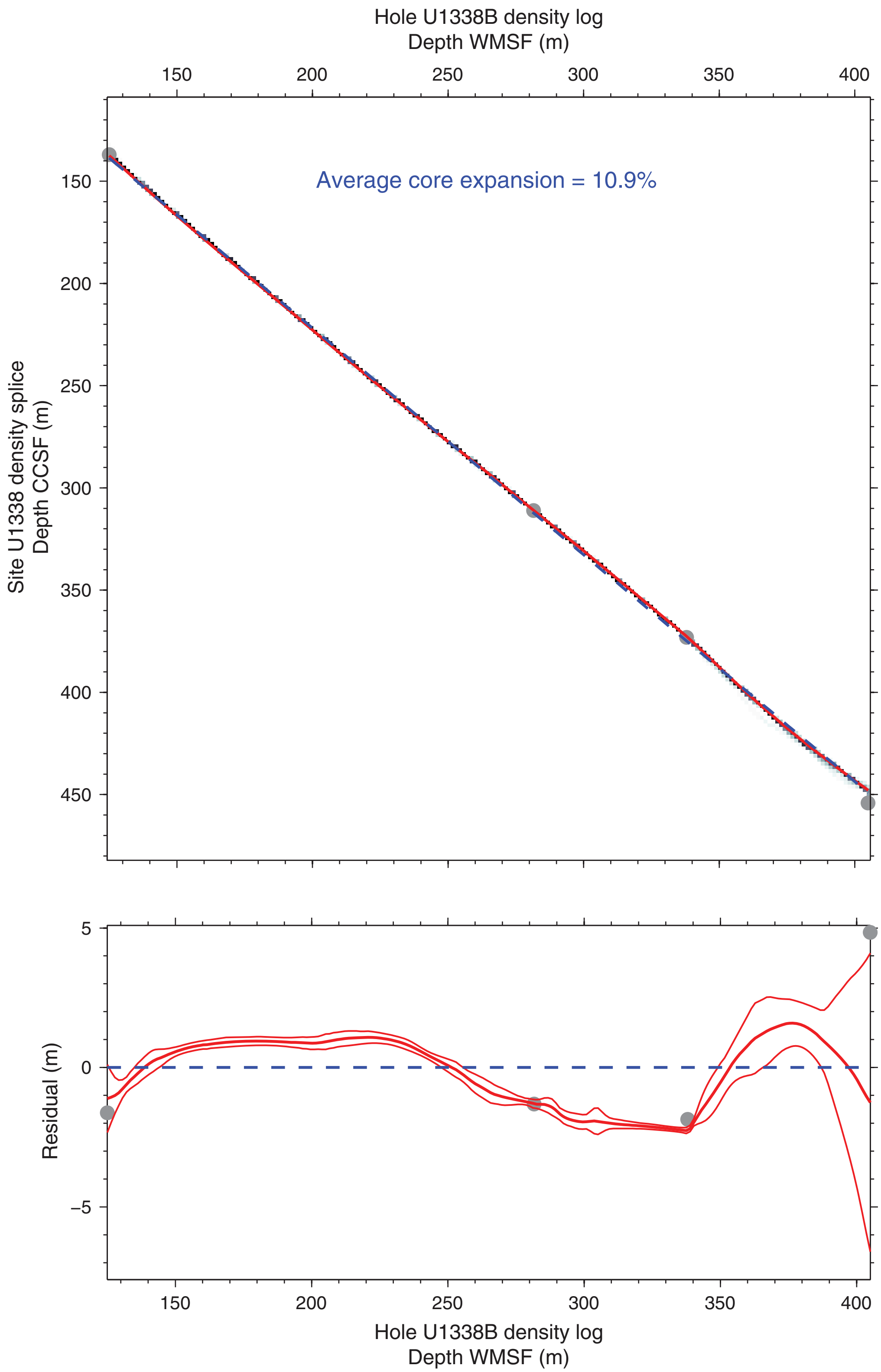

Figure F5. Core splice (red) and downhole log data (black) at Site U1337 plotted on the same depth scale from the mapping function in Figure F3.

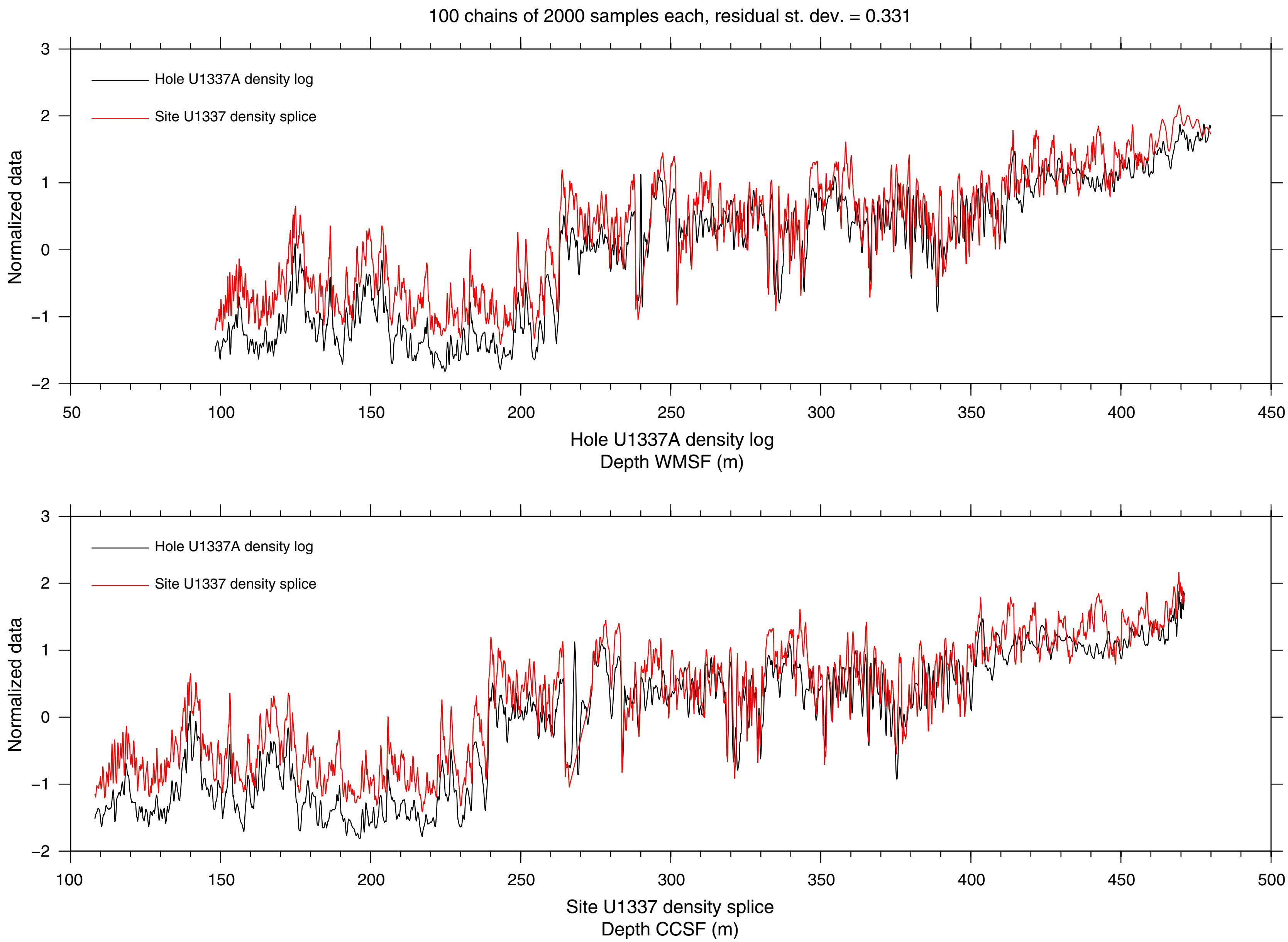

Figure F6. Core splice (red) and downhole log data (black) at Site U1338 plotted on the same depth scale from the mapping function in Figure F4.

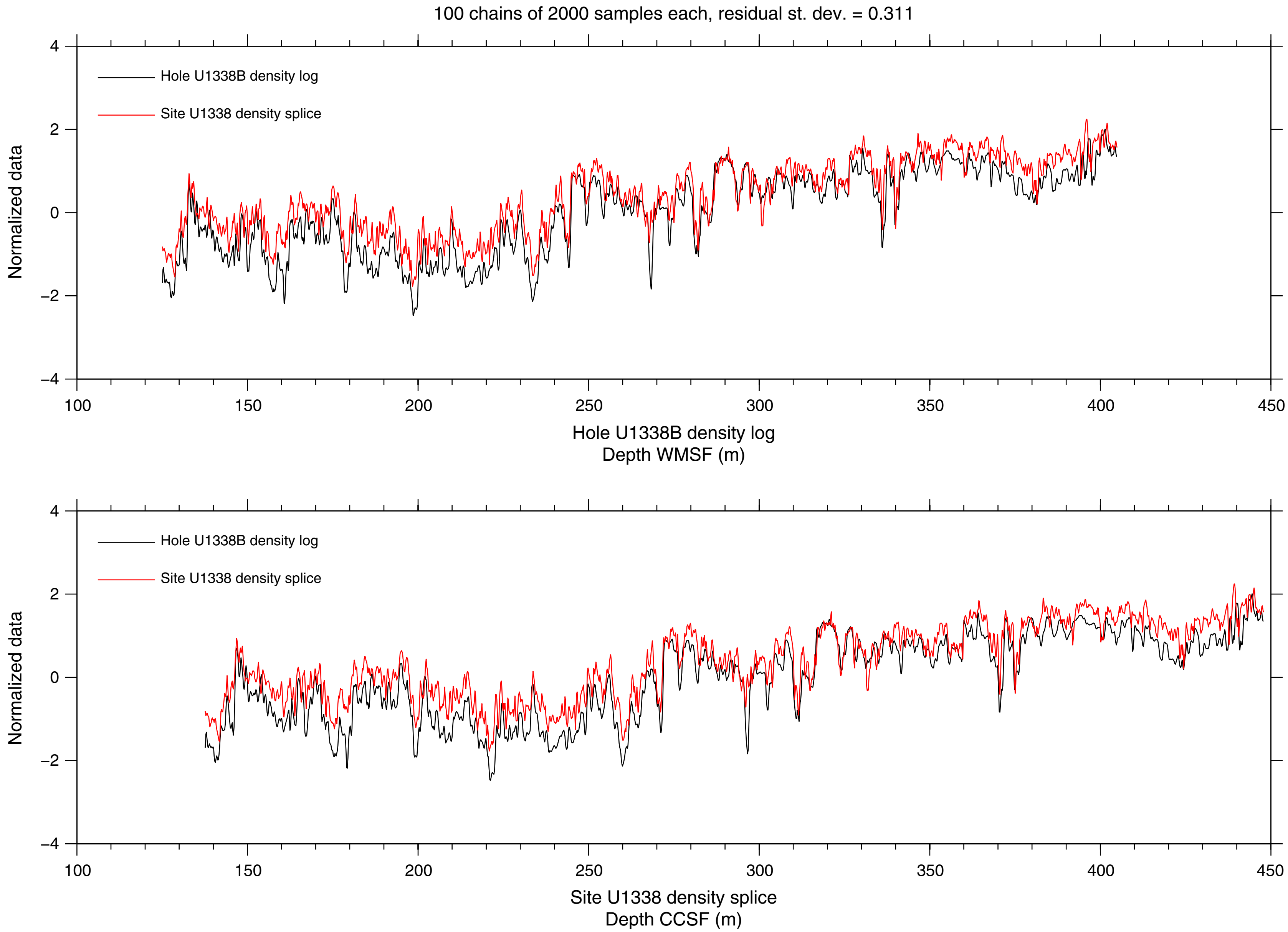

Figure F7. Results of Monte Carlo correlation of core splice records between Sites U1337 (red) and U1338 (black). The core splice data are plotted on the same depth scale (m CCSF at Site U1337 and U1338).

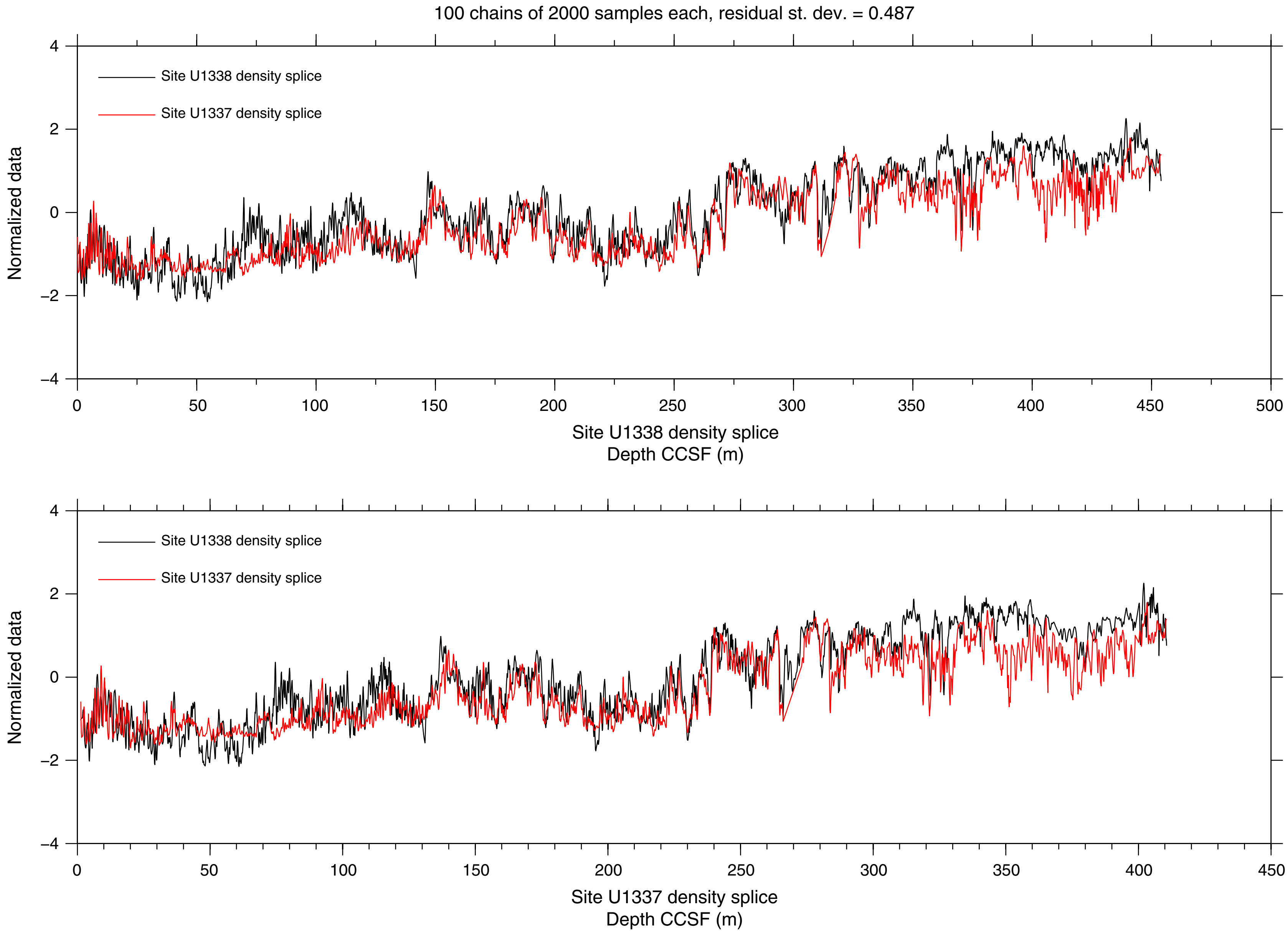

Figure F8. Results of Monte Carlo correlation of downhole log records between Sites U1337 (red) and U1338 (black). The downhole log data are plotted on the same depth scale (m CCSF at Site U1337 and U1338).

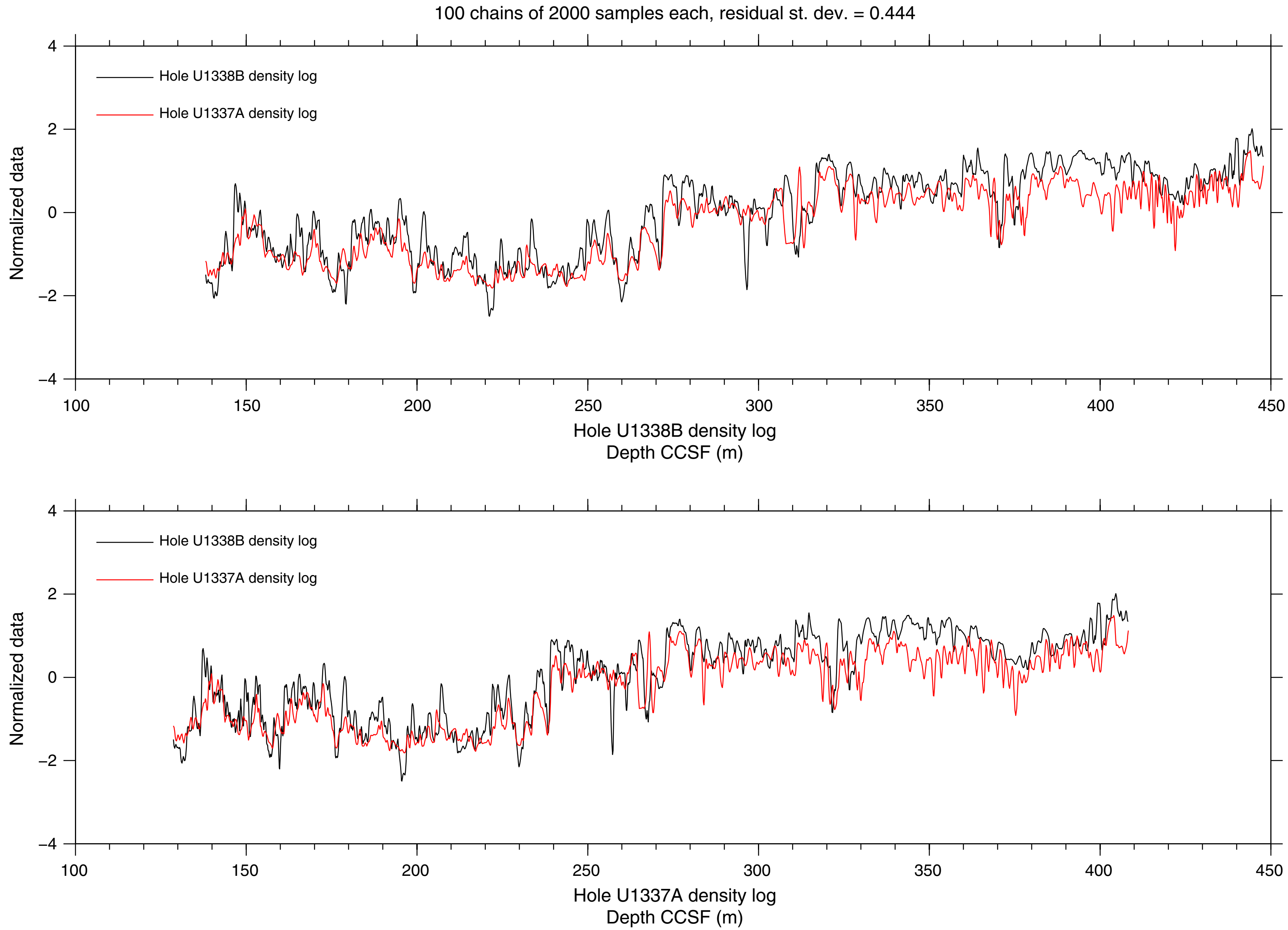

Figure F9. Mapping functions that correlate CCSF depths of core splice (red) and downhole log data (blue) between Sites U1337 and U1338. The light red and light blue regions show the uncertainty bands of the mapping functions (±1 standard deviation).

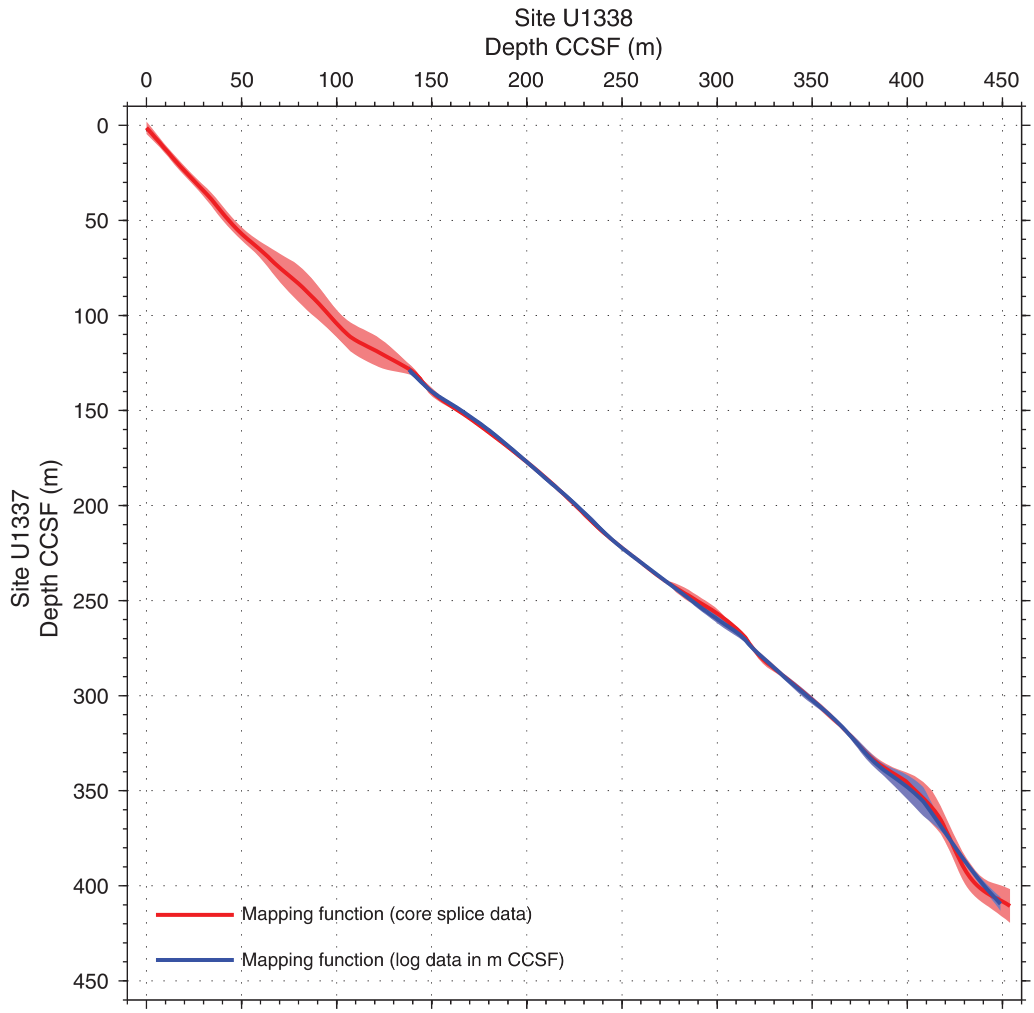

Table T1. Mapping function that correlates depths in the core density splices of Sites U1337 and U1338. (Continued on next page.)

Site U1338 splice depth (m CCSF)	Site U1337 splice depth (m CCSF)	Site U1337 standard deviation (m)
0	1.28388	3.31408
2.28141	3.84603	3.00754
4.56281	6.41747	2.7483
6.84422	9.00798	2.4761
9.12563	11.6412	2.33072
11.407	14.3104	2.30436
13.6884	16.9884	2.41982
15.9698	19.6142	2.58173
18.2513	22.1322	2.56567
20.5327	24.5728	2.46581
22.8141	26.9531	2.46445
25.0955	29.2971	2.59239
27.3769	31.6824	2.72611
29.6583	34.0662	2.97691
31.9397	36.4646	3.23703
34.2211	39.0765	3.48905
36.5025	41.8469	3.73096
38.7839	44.682	3.83419
41.0653	47.4388	3.64707
43.3467	50.0899	3.63056
45.6281	52.6086	3.48884
47.9095	55.0019	3.49701
50.191	57.1852	3.4782
52.4724	59.2051	3.4671
54.7538	61.1676	3.56511
57.0352	63.1005	3.79647
59.3166	65.0634	4.20693
61.598	67.0955	4.77488
63.8794	69.194	5.47067
66.1608	71.3026	6.22947
68.4422	73.4713	6.97877
70.7236	75.5712	7.66733
73.005	77.5344	8.27714
75.2864	79.3701	8.80967
77.5678	81.1948	9.30452
79.8492	83.1502	9.55819
82.1307	85.2876	9.68201
84.4121	87.5345	9.69717
86.6935	89.8244	9.5662
88.9749	92.1395	9.19264
91.2563	94.5385	8.69128
93.5377	97.0311	8.18219
95.8191	99.5897	7.70321
98.1005	102.159	7.37389
100.382	104.678	7.16303
102.663	107.074	7.15388
104.945	109.331	7.36019
107.226	111.239	7.60291
109.508	112.766	7.76307
111.789	114.077	7.87423
114.07	115.269	7.94462
116.352	116.425	7.98157
118.633	117.556	7.95899
120.915	118.726	7.81833
123.196	120.006	7.48026
125.477	121.263	7.1179
127.759	122.485	6.3845
130.04	123.739	5.55726
132.322	124.987	4.79608
134.603	126.256	3.91786
136.884	127.525	3.10163
139.166	128.904	2.42374
141.447	130.641	1.91209
143.729	133.093	1.39506
146.01	135.97	1.56747
148.291	138.693	2.14053
150.573	140.743	2.21325
152.854	142.572	2.01456
155.136	144.328	1.74694
157.417	145.863	1.50946
159.698	147.331	1.31029
161.98	148.795	1.19271
164.261	150.27	1.13018
166.543	151.772	1.13323
168.824	153.316	1.13758
171.106	154.928	1.02027
173.387	156.565	0.935048
175.668	158.253	0.847408
177.95	159.94	0.81594
180.231	161.664	0.812485
182.513	163.426	0.806787
184.794	165.186	0.83375
187.075	166.95	0.954526
189.357	168.72	1.13948
191.638	170.494	1.33343
193.92	172.286	1.39258
196.201	174.099	1.49169
198.482	175.91	1.51038
200.764	177.749	1.53017
203.045	179.634	1.54687
205.327	181.54	1.546
207.608	183.494	1.53044
209.889	185.474	1.54754
212.171	187.497	1.57202
214.452	189.536	1.53381
216.734	191.596	1.52506
219.015	193.694	1.55435
221.296	195.82	1.58287
223.578	197.988	1.58296
225.859	200.197	1.56087
228.141	202.448	1.56452
230.422	204.766	1.58171
232.704	206.997	1.54244
234.985	209.18	1.43417
237.266	211.415	1.4087
239.548	213.565	1.35075
241.829	215.538	1.1786
244.111	217.455	0.969104
246.392	219.351	0.764728
248.673	221.197	0.604229
250.955	222.987	0.463438
253.236	224.755	0.342255
255.518	226.535	0.24922
257.799	228.309	0.187123
260.08	230.078	0.170661
262.362	231.85	0.182373
264.643	233.621	0.176838
266.925	235.39	0.187012
269.206	237.15	0.19184
271.487	238.892	0.175212
273.769	240.379	0.780353
276.05	241.821	1.57368
278.332	243.271	2.24466
280.613	244.698	2.65889
282.894	246.113	2.9839
285.176	247.497	3.0751
287.457	248.888	3.01314
289.739	250.329	2.96357
292.02	251.796	2.98039
294.302	253.128	2.88875
296.583	254.492	2.73647
298.864	255.916	2.5327
301.146	257.527	2.10323
303.427	259.256	1.5386

Table T1 (continued).

Site U1338 splice depth (m CCSF)	Site U1337 splice depth (m CCSF)	Site U1337 standard deviation (m)
305.709	261.048	0.994405
307.99	262.908	0.530724
310.271	264.867	0.184158
312.553	266.98	0.679106
314.834	269.445	1.02094
317.116	272.787	1.11626
319.397	275.827	1.55318
321.678	278.464	2.01858
323.96	280.767	2.35361
326.241	282.757	2.3623
328.523	284.546	2.0471
330.804	286.361	1.69418
333.085	288.17	1.41619
335.367	289.992	1.2607
337.648	291.852	1.28611
339.93	293.722	1.46453
342.211	295.598	1.52835
344.492	297.494	1.58839
346.774	299.408	1.52345
349.055	301.338	1.51983
351.337	303.324	1.59476
353.618	305.311	1.73181
355.899	307.318	1.87858
358.181	309.385	1.91266
360.462	311.514	1.79407
362.744	313.676	1.56884
365.025	315.859	1.18507
367.307	318.107	1.12235
369.588	320.487	1.34326
371.869	323.015	1.78777
374.151	325.592	2.17731
376.432	328.24	2.3615
378.714	330.71	2.50114
380.995	332.819	2.56814
383.276	334.6	2.4592
385.558	336.255	2.38882
387.839	337.795	2.43229
390.121	339.282	2.72114
392.402	340.718	3.04723
394.683	342.084	3.51293
396.965	343.474	4.06877
399.246	345.058	4.75506
401.528	347.128	5.90653
403.809	349.429	7.1415
406.09	351.809	8.10669
408.372	354.004	8.58024
410.653	356.231	8.78619
412.935	358.726	8.72905
415.216	361.744	8.07842
417.497	365.319	7.2966
419.779	369.666	6.90547
422.06	374.539	6.75152
424.342	379.513	6.88071
426.623	384.391	7.07593
428.905	389.02	7.27034
431.186	393.111	7.47794
433.467	396.293	7.36256
435.749	398.789	6.89603
438.03	401.076	6.58076
440.312	402.83	6.53528
442.593	404.295	6.7088
444.874	405.567	7.07006
447.156	406.73	7.54732
449.437	407.896	8.04927
451.719	409.227	8.44684
454	410.627	8.92487

This mapping function is plotted in Figure F9. The three columns contain the depth at Site U1338 (m CCSF), the correlated depth at Site U1337 (m CCSF), and the uncertainty in correlated depth at Site U1337 (1 standard deviation [m]).

Table T2. Mapping function that correlates depths converted to m CCSF in the downhole density logs of Sites U1337 and U1338. (Continued on next page.)

Site U1338 log depth (m CCSF)	Site U1337 log depth (m CCSF)	Site U1337 standard deviation (m)	Site U1338 log depth (m CCSF)	Site U1337 log depth (m CCSF)	Site U1337 standard deviation (m)
138	128.559	2.07607	242.709	216.125	1.33528
139.563	130.156	1.65262	244.271	217.535	1.21543
141.126	131.746	1.25769	245.834	218.889	1.09118
142.688	133.325	0.918699	247.397	220.187	0.97938
144.251	134.896	0.712893	248.96	221.456	0.876122
145.814	136.445	0.738443	250.523	222.709	0.78304
147.377	137.886	0.886192	252.085	223.929	0.696907
148.94	139.209	1.07082	253.648	225.128	0.613717
150.503	140.425	1.21886	255.211	226.321	0.541264
152.065	141.556	1.30077	256.774	227.507	0.475552
153.628	142.585	1.24014	258.337	228.686	0.409684
155.191	143.568	1.14488	259.899	229.865	0.352471
156.754	144.538	1.05357	261.462	231.047	0.297974
158.317	145.493	0.963895	263.025	232.227	0.245284
159.879	146.444	0.86491	264.588	233.405	0.206861
161.442	147.412	0.748289	266.151	234.587	0.16785
163.005	148.402	0.627226	267.714	235.774	0.148588
164.568	149.413	0.504916	269.276	236.961	0.17027
166.131	150.439	0.420832	270.839	238.149	0.208887
167.693	151.495	0.359971	272.402	239.338	0.272797
169.256	152.573	0.319189	273.965	240.51	0.347421
170.819	153.667	0.323905	275.528	241.673	0.425237
172.382	154.772	0.377227	277.09	242.831	0.509714
173.945	155.893	0.459405	278.653	243.994	0.606631
175.508	157.014	0.568588	280.216	245.164	0.735092
177.07	158.155	0.691072	281.779	246.335	0.879865
178.633	159.321	0.817906	283.342	247.523	1.03179
180.196	160.532	0.90395	284.905	248.716	1.20972
181.759	161.777	0.882583	286.467	249.912	1.40416
183.322	163.028	0.838265	288.03	251.11	1.60371
184.884	164.27	0.813164	289.593	252.274	1.66458
186.447	165.534	0.759095	291.156	253.417	1.73429
188.01	166.829	0.70772	292.719	254.545	1.80647
189.573	168.138	0.742354	294.281	255.668	1.87287
191.136	169.456	0.835022	295.844	256.763	1.90536
192.698	170.79	0.961559	297.407	257.844	1.9756
194.261	172.137	1.09583	298.97	258.945	2.08692
195.824	173.467	1.1459	300.533	260.044	2.23057
197.387	174.807	1.15388	302.095	261.12	2.32344
198.95	176.177	1.14531	303.658	262.156	2.33463
200.513	177.549	1.1646	305.221	263.179	2.31632
202.075	178.911	1.18783	306.784	264.253	2.26928
203.638	180.268	1.23973	308.347	265.333	2.22659
205.201	181.627	1.31885	309.91	266.425	2.11666
206.764	182.985	1.41871	311.472	267.558	1.95534
208.327	184.341	1.48215	313.035	268.9	1.74957
209.889	185.683	1.45326	314.598	270.502	1.45194
211.452	187.03	1.42295	316.161	272.332	1.05539
213.015	188.383	1.38628	317.724	274.061	0.830873
214.578	189.737	1.35069	319.286	275.666	0.750716
216.141	191.097	1.32165	320.849	277.16	0.777198
217.704	192.464	1.30171	322.412	278.595	0.89076
219.266	193.84	1.2794	323.975	279.994	1.04636
220.829	195.231	1.26414	325.538	281.381	1.19839
222.392	196.633	1.26202	327.101	282.788	1.24821
223.955	198.078	1.27643	328.663	284.192	1.29646
225.518	199.53	1.33012	330.226	285.589	1.33462
227.08	200.971	1.35111	331.789	286.984	1.39996
228.643	202.418	1.4043	333.352	288.361	1.45146
230.206	203.877	1.48772	334.915	289.73	1.53371
231.769	205.375	1.58104	336.477	291.081	1.64079
233.332	206.903	1.68751	338.04	292.43	1.75401
234.894	208.464	1.73471	339.603	293.767	1.87392
236.457	210.042	1.69035	341.166	295.106	1.99472
238.02	211.609	1.60061	342.729	296.426	2.09854
239.583	213.171	1.51723	344.291	297.725	2.14584
241.146	214.678	1.44541	345.854	299.019	2.15013

Table T2 (continued).

Site U1338 log depth (m CCSF)	Site U1337 log depth (m CCSF)	Site U1337 standard deviation (m)
347.417	300.325	2.12465
348.98	301.613	2.0702
350.543	302.881	1.96528
352.106	304.158	1.85214
353.668	305.451	1.71848
355.231	306.758	1.55984
356.794	308.083	1.41159
358.357	309.453	1.27114
359.92	310.845	1.17262
361.482	312.248	1.11332
363.045	313.687	1.08874
364.608	315.178	1.14855
366.171	316.781	1.22427
367.734	318.492	1.28519
369.296	320.247	1.44276
370.859	322.012	1.70079
372.422	323.79	1.97364
373.985	325.563	2.23835
375.548	327.354	2.43888
377.111	329.146	2.58955
378.673	330.853	2.70302
380.236	332.513	2.77065
381.799	334.114	2.7947
383.362	335.562	2.76912
384.925	336.881	2.82989
386.487	338.178	2.97809
388.05	339.375	3.22442
389.613	340.517	3.57737
391.176	341.644	3.98811
392.739	342.761	4.43956
394.302	343.866	4.86641
395.864	344.98	5.32245
397.427	346.103	5.78197
398.99	347.319	6.13892
400.553	348.564	6.50022
402.116	349.868	6.83795
403.678	351.241	7.10652
405.241	352.66	7.35654
406.804	354.096	7.55206
408.367	355.677	7.56879
409.93	357.684	6.9196
411.492	359.842	5.98716
413.055	362.005	5.07058
414.618	364.192	4.19774
416.181	366.428	3.39033
417.744	368.756	2.59916
419.307	371.116	1.86949
420.869	373.523	1.38022
422.432	375.947	1.21128
423.995	378.194	1.13829
425.558	380.39	1.06387
427.121	382.581	1.07832
428.683	384.771	1.18883
430.246	386.928	1.32372
431.809	389.052	1.48439
433.372	391.164	1.68305
434.935	393.244	1.87712
436.497	395.262	2.01522
438.06	397.233	2.10228
439.623	399.129	2.17404
441.186	400.937	2.29032
442.749	402.698	2.45713
444.312	404.42	2.64912
445.874	406.126	2.91616
447.437	407.851	3.2303
449	409.577	3.59081

This mapping function is plotted in Figure **F9**. The three columns contain the depth at Site U1338 (m CCSF), the correlated depth at Site U1337 (m CCSF), and the uncertainty in correlated depth at Site U1337 (1 standard deviation [m]).